Dual Band, Miniaturized, Implantable Antenna Design with On-body Antennas for Wireless Health Monitoring

Ademola O. Kaka [1], Mehmet Toycan [1], Stuart D. Walker [2], and Doğa Kavaz [3]

[1] Cyprus International University, Faculty of Engineering, Department of Electric and Electronic Engineering
Nicosia, Northern Cyprus, Mersin 10, Turkey
mtoycan@ciu.edu.tr

[2] School of Computer Science and Electronic Engineering, University of Essex, Colchester, UK

[3] Cyprus International University, Faculty of Engineering, Bioengineering Department
Nicosia, Northern Cyprus, Mersin 10, Turkey
dkavaz@ciu.edu.tr

Abstract ─ A modified Hilbert fractal geometry and serpentine radiator-based implant antenna is proposed for dual band medical operations in both the MICS band (402-405 MHz) and ISM band (2.4–2.48 GHz). The antenna has miniaturized dimensions of 5.5 x 7.6 x 0.8 mm^3 (width x height x thickness) and is simulated inside a four layer (air, skin, fat and muscle) model with dimensions of 150 mm x 75mm x 55 mm. A Zirconia (ε_r=29) superstrate and shorting pin were utilized to achieve biocompatibility and the desired resonance. Relatively stable and omni-directional radiation patterns were achieved for the dual band operation. An ISM band on-body antenna (5.8 x 5.5 x 0.8 mm^3) was proposed to generate a wake-up signal while the wireless telemetry transmission was achieved using the MICS band on-body antenna (5.8 x 5.5 x 0.8 mm^3). Implant and on-body antennas demonstrated a reflection coefficient (S_{11}) better than -10 dB characteristics. To adhere to the SAR regulation limit of 1.6W/kg, the peak incident power should not exceed 0.25 mW and 0.2 mW for the ISM band and MISC band on-body antennas respectively. Propagation channel characteristics were simulated by observing the S_{12} and S_{13} characteristics and satisfactory results were achieved. The peak gain for the implant, MICS band and ISM band on-body antennas were -39.8 dBi, -35.6 dBi and -23 dBi, respectively due to the miniature dimensions. The miniaturized characteristics, dual-band operation, biocompatibility and stable characteristics in the presence of human tissue model make both the implant and on-body antennas suitable for biomedical monitoring systems.

Index Terms ─ Biocompatible, dual-band, implant antenna, miniaturized, on-body antenna.

I. INTRODUCTION

Wireless Body Area Network systems (WBANs) have great potential in a wide range of applications including health-monitoring, mobile-health, military etc., for the collection of real-time and stored physiological data [1,2]. Communication channels of WBANs are typically categorized as in-, on-, and off-body [3]. Implant antennas have a vital role for the provision of a high-quality communication link between the in-body and on-body medical units [4-8]. Compared to well-known antenna design techniques, implantable antennas should be miniaturized for physiological acceptability. In addition, these implants have some unique challenges with regards to impedance matching, bandwidth, multiband operation, low-power requirements (specific absorption rate limitation) and biocompatibility due to the variation in the electrical properties of human body tissues [6]. As demonstrated in previous studies, antenna characteristics must be optimized to achieve acceptable performance by accounting for detuning effects inside the human body which may otherwise have a considerable impact on the antenna response [9]. The implant antenna should possess satisfactory transmission characteristics in order to function as the communication link between an implanted device and an exterior instrument for biotelemetry. The Medical Implant Communications Service (MICS) band (402–405 MHz) is mainly used as the transmission channel between the implant unit and the on- or off-body units and is regulated by the United States Federal Communications Commission (1999) and the European Radio Communications Committee (1997). There is also an opportunity to operate in the Industrial, Scientific and Medical (ISM) bands of 915, 2450 and 5800 MHz

Submitted On: December 13, 2019
Accepted On: April 12, 2020

(Federal Communications Commission, 2012) to activate the implant medical unit [10]. An implant device may be switched between sleep and active modes to realize improve efficiency and extend the battery life of the device [11]. A raft of simulations for one- or three-layer tissue models have been proposed for the realization of in-depth analysis for surrounding complicated tissue environment [9,12] and subsequent experiments have investigated tissue-equivalent liquids [5,7], mimicking gels [11], and animals [13]. Several antenna designs have also been proposed with broadband and dual-band characteristics [14-18].

Antennas with dual band operation, in the MICS and ISM frequency bands, are achieved using Serpentine curves in [11-13] which have dimensions of 22.5 x 22.5 x 2.5 mm^3. Another antenna with smaller dimensions, 15Ã—22.5Ã—2.5 mm^3, can be used with a multilayer configuration and includes an independent line to feed radiating elements via electromagnetic coupling [12]. While this approach allows for greater miniaturization, the bandwidth requires further improvement. The Sierpinski fractal concept was utilized for Planar Inverted-F Antenna (PIFA) to achieve dual-band transmission [16] and a dual-band textile antenna based on Half-Mode Substrate Integrated Waveguide (HMSIW) in has been realized, albeit with a large form factor [18]. Circularly polarized (CP) radiation is usually preferred to linearly polarized radiation for wireless telemetry applications due to the reduced multipath and an improved bit error rate [19]. On-body antennas should also be designed with simple, flexible, miniaturized and reduced radiation characteristics. The gain of these antennae are typically reduced due to the proximity to human tissues [20]. Multiple antenna designs in the literature have also been proposed for WBAN applications [21-26].

The proposed implant antenna has a miniaturized size making it suitable for placement into an arm of the human body model. A three layer tissue model (skin, fat and muscle) which was also used in [9] is used in this research study. The radiating patch of the implant antenna is characterized using a combination of Hilbert fractal and serpentine geometries to realize dual-band operation and satisfactory transmission characteristics inside the arm model. Self-similarity and space filling are the two unique characteristics of Hilbert and serpentine geometries which allow for longer electrical lengths while maintaining the reduced physical size of the radiating patch. These characteristics allow for miniaturization and enhance resonances at the desired frequencies. Kaka et al. (2012) characterized the geometric generation and configuration of the Hilbert fractal geometry-based implant antenna [27]. Zirconia is used as a superstrate material in order to achieve biocompatible properties while preventing direct contact between the implant and human tissue. Along with the proposed implant antenna, on-body antennas for MICS and ISM bands are designed using hexagonal and circular serpentine geometries accordingly.

The first objective is to simulate the proposed implant antenna inside the three-layer human arm model phantom for dual band operation. As a second design objective, the two on-body antennas are characterized and the path loss is analysed. The design methodology of the implant and on-body antennas is introduced in Section 2. Antenna geometry parameterizations are presented in Section 3. Various simulated performance analysis, including return loss, axial ratio and radiation characteristics, are discussed in Section 4. Conclusions are given in Section 5.

II. DESIGN METHODOLOGY OF IMPLANT AND ON-BODY ANTENNAS

The four-step design methodology applied in this research study is shown in Fig. 1. First, the implant antenna was characterized and placed inside a human arm model with dimensions 150 x 75 x 55 mm^3 (width × height × thickness mm^3) for the purpose of determining transmission characteristics, in particular reflection coefficient (S_{11}) values. Modifications are then made on the Hilbert and Serpentine geometries to achieve dual band operation with satisfactory transmission characteristics. S_{11} results better than -10 dB are acceptable for transmission.

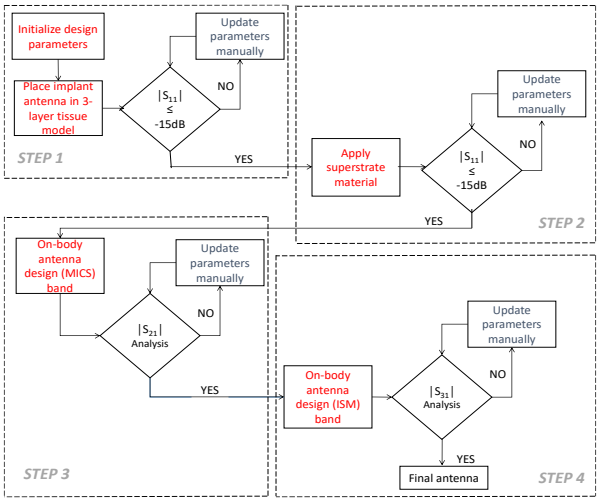

Fig. 1. Proposed generic four–step methodology for implantable antenna design.

The second objective (Step 2) was to consider a superstrate dielectric layer to achieve biocompatible characteristics while preventing direct contact between the implant and human tissues. Additionally, a superstrate can prevent short circuit of the antenna operation by tissue. Some well-known materials that could be used for this approach include Teflon (permittivity – ε_r=2.1; dielectric loss tangent – tan δ=0.001), MACOR

(permittivity – ε_r=6.1; dielectric loss tangent – tan δ=0.005), and ceramic alumina (permittivity – ε_r=9.4; dielectric loss tangent – tan δ=0.006) [1]. The primary challenge here is to select a low-loss, biocompatible material that can insulate the antenna implant with as a thin coating. For this approach, zirconia (permittivity – ε_r=29; dielectric loss tangent – tan δ=0.001) was considered as materials with higher permittivity also resonate at lower frequencies due to shorter effective wavelength [9]. An important research objective in the development of WBAN is to understand the propagation channel characteristics as an essential requirement for the efficient design of wireless communication systems. The third (Step 3) and fourth objectives (Step 4) were to consider the design of on-body antenna designs for both the MICS and ISM bands so that a communication implant with the proposed implant antenna may be realized, as can be seen in Fig. 2. Anatomical tissue models, with the electrical properties of human body tissues, are proposed in the literature [1-3, 5-9, 11-14 and 28]. The proposed antenna in reference [28] is assumed to be implanted subcutaneously into the human model between the shoulder and the elbow with model dimensions of 180 mm x 60 mm x 60 mm. Grey layer, brown layer, green layer and blue layer represents muscle, fat, skin and air layers accordingly. In order to obtain more realistic results in the research study, a four-layer human arm model was used (air, skin, fat and muscle) with the dimensions of 150 mm x 75mm x 55 mm (width × height × thickness mm^3).

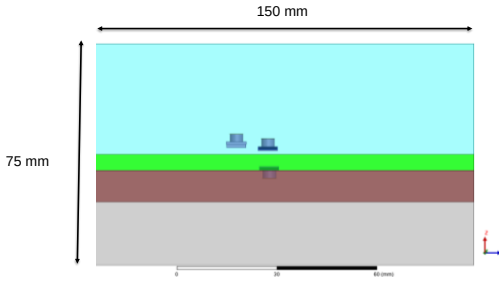

Fig. 2. Propagation channel characteristics for dual band operation from implant antenna to on-body antennas. Grey, brown, green and blue represent muscle, fat, skin, and air, respectively.

III. PROPOSED ANTENNA GEOMETRY PARAMETERIZATION

A. Implant antenna parameterization

Three layers were used to design the proposed antenna: layer 1 was used as a ground plane and layer 2 was characterized as a radiating element. A superstrate material was applied in layer 3 realization of biocompatibility. The final implant antenna geometry, a 3D render of the proposed antenna design, and the three-layer human tissue model that was used to simulate antenna performance, are depicted in Figs. 3 (a), (b) and (c), respectively. Rogers R03010 was used as the substrate with a dielectric constant (ε_r) of 10.2 and loss tangent (tan δ) of 0.0035. The thickness of the substrate was 0.9 mm and the feed position is located at the centre (*xy*-axis) of the structure as depicted in Fig. 3 (b).

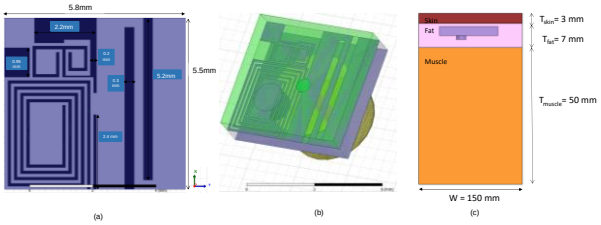

Fig. 3. (a) Final antenna geometry, (b) 3D of proposed antenna design, and (c) three-layer human tissue model.

As can be seen from Figs. 3 (a) and (b), two major design guidelines, Hilbert fractal geometry and serpentine geometry, were applied to achieve the proposed antenna's radiating element geometry. The initial shape of a square was used due to its ease of modification and the fact it is centro-symmetric on (0, 0). The initial square was divided into two vertical sections on the x-axis and a Hilbert fractal geometry modification was applied to the top left of the half-square region. The Hilbert generation process has previously been considered in [27] and the original first iteration modified by removing the right top part of the geometry. The serpentine geometry was applied beneath the Hilbert fractal geometry in order to increase the capacitive nature of the design [9]. The modification for the left-most region was intended to achieve resonance for MICS bandwidth. By utilizing modifications on the left-part of the square, a longer electrical length was achieved resulting in resonance at lower frequencies. Finally, two slits were removed from the centre of the right-part of the square in order to achieve resonance for the ISM bandwidth.

A shorting pin with a radius of 0.5 mm was used at the centre of the serpentine geometry, as seen in the left-part of the design in Fig. 3 (b), to connect radiating elements with the ground plane. This application causes an increase in the effective size of the antenna while also enhancing resonances on the desired frequencies [6]. A coaxial probe is employed as a feeding line and proposed implant antenna parameters were characterized to achieve 50 ohm impedance matching. Figure 3 (b) depicts the Zirconia superstrate material in green (thickness of 0.5 mm) which was used to prevent direct the contact of human tissue by the implant. A three layer tissue model (skin, fat and muscle) was used as a simulation environment with similar electrical characteristics as human arm model. As depicted in Fig. 3 (c), this model has dimensions 150 × 75 × 60 mm^3 (width × height × thickness). The electrical properties of each layer are

specified in Table 1 at 433 MHz and 2.45 GHz. It should be noted that the values are defined by the Office of Engineering and Technology (OET Bulletin 65 Supplement C) of the FCC (2001) [29].

As fat tissue exhibits lower loss characteristics than skin and muscle, the proposed implant was placed into a fat layer at a depth of 5 mm from the surface of the skin [9]. As Zirconia has a higher conductivity than human tissue, the MICS bandwidth resonance is enhanced.

Table 1: Electrical properties of body tissue at the different frequency bands [29]

	Relative Permittivity ε_r		Conductivity σ (S/m)	
Frequency (MHz)	433	2450	433	2450
Body equivalent tissue	56.7	52.7	0.94	1.95
Skin	46.08	38.01	0.7	1.46
Fat	5.57	5.28	0.04	0.1
Muscle	56.87	52.73	0.8	1.74

B. MICS band on-body antenna parameterization

The proposed on-body antenna for operation at the MICS bandwidth was realized using two design concepts. The antenna was designed on a rectangular Roger RO3010 substrate with a dielectric constant (εr) of 10.2 and loss tangent (tan δ) of 0.0035. First, a serpentine geometry was applied on a hexagonal geometry and Zirconia material was applied as a superstrate to shield all sides of the patch and achieve resonance in the desired MICS bandwidth which is necessary due to the higher permittivity of human tissue. Probe-feed excitation device was placed at the centre of the radiator. The initial design geometry is illustrated in Fig. 4 (a) and dimensions are presented in Table 2. The substrate thickness is 0.8 mm and the total antenna size is 6 × 5.7 x 1.3 mm^3 (width × height x thickness). The top layer superstrate thickness is 0.5 mm while the two sides are 0.1 mm each and dark blue area superstrate thickness applied is 5.6 mm.

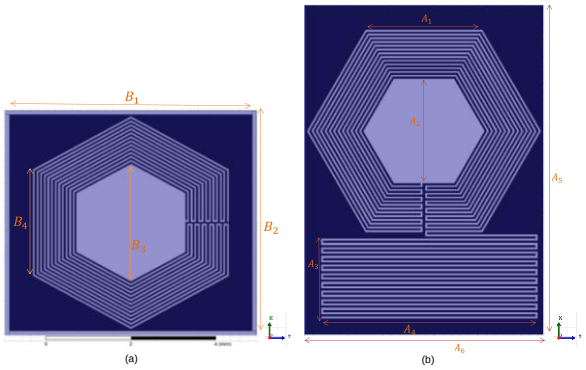

Fig. 4. (a) Initial design geometry of the MICS band on-body antenna, and (b) final design geometry with further increased electrical length.

Table 2: MICS band on-body antenna initial design parameters

Parameters (mm)	B_1	B_2	B_3	B_4
	6	5.7	3	2.7

As a result of the shielding effect and the high electrical permittivity of the Zirconia superstrate, it was observed that the antenna experiences poor radiation efficiency and increased path-loss. The superstrate was removed from the final design geometry in an attempt to rectify these issues and improve the antenna transmission properties, reduce path-loss characteristics and simplify the structure. In addition to this, electrical path length was increased by applying additional rectangular serpentine geometry beneath the hexagonal shape, as shown in Fig. 4 (b). This resulted in lower resonating frequencies as in line with the outcome from first design concept. The final design antenna parameterization is shown in Table 3 with the dimension 5.5 x 7.6 x 0.8 mm^3 (width × height × thickness).

Table 3: MICS band on-body antenna final design parameters

Parameters (mm)	A_1	A_2	A_3	A_4	A_5	A_6
	2.7	2.725	1.95	5	7.6	5.5

C. ISM-band on-body antenna parameterization

The second proposed on-body antenna that operates at the ISM bandwidth was achieved by applying concentric circles slots within a square-form radiator as shown in Fig. 5. The mathematical expression for circular concentricity is shown in equation (1) where *(h,k)* represents the coordinates of the antenna geometry's centre, *r* is the radius of the most inner circle and r_1 is the radius of the second circle. The concentric design was deployed to increase the antenna's electrical length:

$$(x-h)^2+(y-k)^2 = r^2 \; is \; (x-h)^2+(y-k)^2 = r_1^2, (r_1 \neq r). \quad (1)$$

The antenna was again designed on a rectangular Roger RO3010 substrate. The probe-feed excitation device is placed at the centre of the radiator. The central position of the probe is intended to ensure that the probe size has no impact on the spatial dimension of the patch antenna.

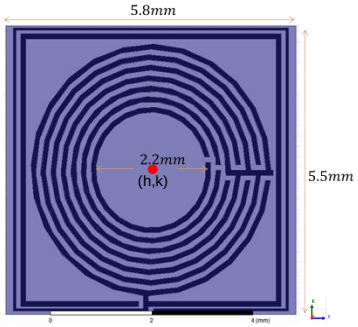

Fig. 5. Design geometry of the ISM band on-body antenna.

IV. SIMULATION RESULTS

Numerical Finite Element Methods (FEM) were applied for the analysis of transmission characteristics of the implant and on-body antennas using commercially available full-wave 3D Ansoft HFSS software. Boundary conditions and meshing of the proposed antennas were chosen with respect to the resonant frequencies with perceived boundary wavelengths. In order to achieve lower resonant frequencies, the use of a dielectric substrate with high permittivity is required in order to achieve shorter effective wavelengths. Electric field distribution for the dual band operation implant antenna is shown in Fig. 6.

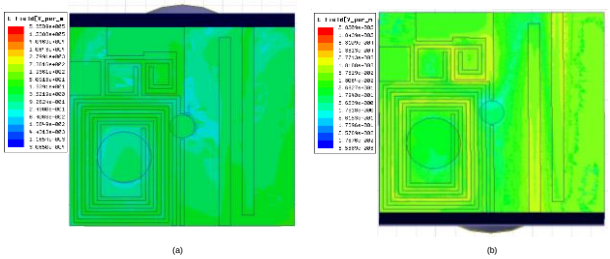

Fig. 6. Implant antenna electric field distribution (a) MICS band and (b) ISM band.

It could be seen from Fig. 6 that the modified Hilbert and serpentine radiator (left hand side of the antenna) was primarily used to achieve a frequency resonance in the MICS band while the two slits on the right-hand side are for the ISM band as expected. There are, however, coupling effects between both radiators. With the help of this dual-band operation, the antenna may be controlled to enter sleep or wake-up modes. The antenna is expected to communicate on MICS bands as soon as a wake-up signal is received in the ISM band. Such an implant would then have improved energy efficiency and a longer life cycle. Figures 7 (a) and (b) display the implant antenna current distribution at MICS and ISM bands respectively showing the same achievement for antenna resonances.

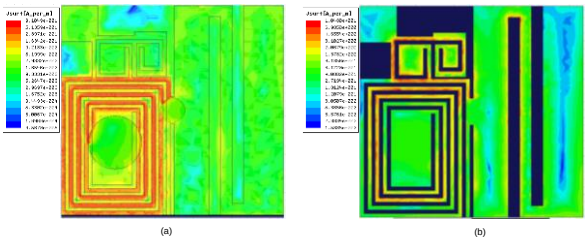

Fig. 7. Implant antenna current distribution (a) MICS band and (b) ISM band.

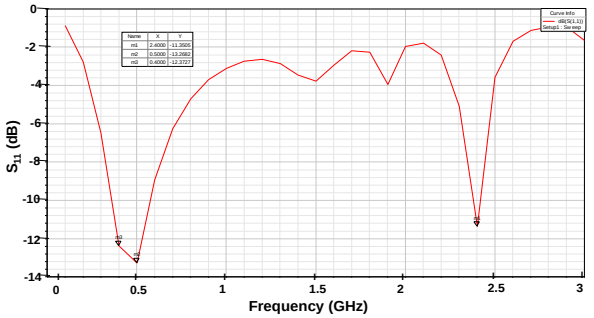

(a)

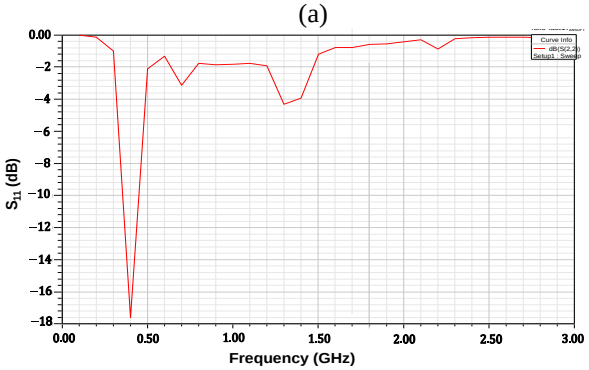

(b)

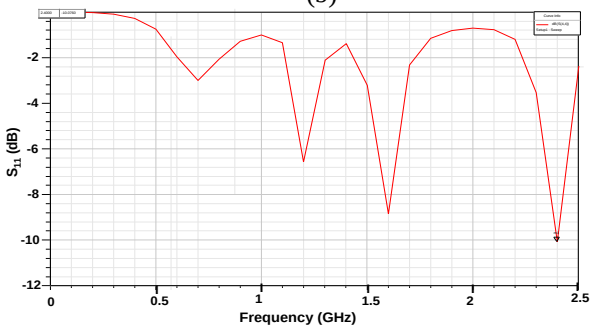

(c)

Fig. 8. Monitoring S_{11} characteristics of (a) proposed antenna with dual band operation, (b) MICS (402-405 MHz) band on-body antenna, and (c) ISM (2.4-2.48 GHz) band on-body antenna.

Figure 8 depicts the simulation analysis of the proposed implant and on-body antenna performances by monitoring simulated reflection coefficient (S_{11}) variations over the transmission bandwidths. It should be noted that the simulation of reflection coefficient analysis of the implant antenna over the MICS (402-405 MHz) and ISM (2.4–2.48 GHz) bands are achieved at the same time and that reflection coefficient characteristics are enhanced with S_{11} below -10 dB as shown in Fig. 8 (a). In addition, the analysis of the MICS and ISM band on-body antennas reveal satisfactory reflection coefficient characteristics as shown in Figs. 8 (b) and (c)

respectively. Voltage Standing Wave Ratio (VSWR) simulation results of the proposed implant antenna and on-body antennas, over transmission bandwidths, are less than 2. These results indicate satisfactory matching characteristics and correlate with the reflection coefficient measurements.

The real and imaginary parts of the input impedance as a function of proposed implant antenna frequency, MICS band on-body antenna and ISM band on-body antenna are shown in Figs. 9 (a), (b) and (c) respectively.

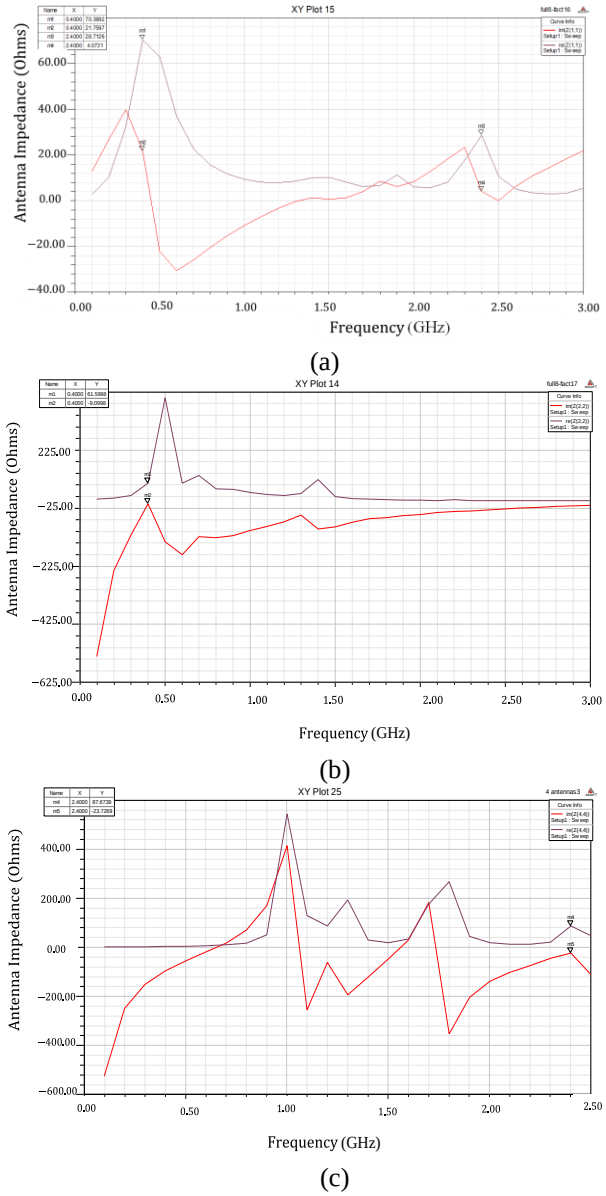

Fig. 9. Input impedance of (a) proposed implant antenna, (b) MICS band on-body antenna, and (c) ISM band on-body antenna: real part (purple line) and imaginary part (red line) over MICS and ISM bands.

It can be observed from Fig. 9 (a) that at the resonance frequency of 400 MHz, the real part of the input impedance is approximately 70 Ω, which is in line with a reflection coefficient of better than -10 dB and an acceptable level for communication. However, the imaginary part is far from zero at 21 Ω. For the ISM band, the real and imaginary parts are approximately 28 Ω and 4 Ω, respectively. On-body antennas can be matched to an approximately 50 Ω line for the mono-band and dual band operations bandwidth. A matching circuit can be used in practice to realize stable 50 Ω matching.

Figures 10 (a) and (b) illustrates the 3D radiation patterns for the 400 MHz and 2.4 GHz resonance frequencies, respectively. Omni-directional radiation properties, with a toroidal shape, were seen in both H-plane and in the E-plane for dual-band operation. Hence, accurate orientation alignment is demonstrated.

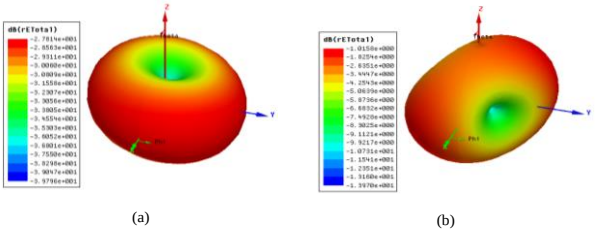

Fig. 10. 3D simulated radiation patterns of the proposed implant antenna at (a) 400 MHz and (b) 2.4 GHz.

Specific Absorption Rate (SAR) is a vital measure of rate and which must adhere to the FCC approved limit [9]. Based on the HFSS simulations, a 10g average SAR from the arm model is given at 105W/kg at 400 MHz and 464 W/kg at 2.4 GHz. It should be noted that SAR values were achieved under a 1W input power condition, illustrated in Fig. 11 for dual band operation. In accordance, the incident power for the proposed implant antenna should be lower than 15.2 mW and 3.4 mW for the MICS and ISM bands, respectively, in order to meet the 1.6 W/kg regulation limit.

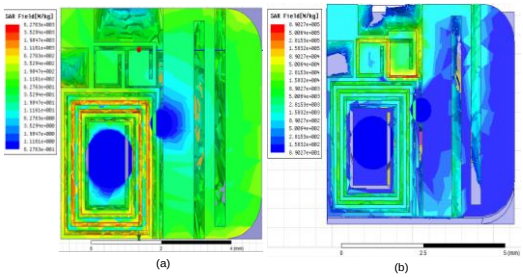

Fig. 11. Proposed implant antenna showing the electromagnetic energy (SAR profile) distribution at (a) 400 MHz and (b) 2.4 GHz.

In addition, SAR characteristics of the on-body antennas (MICS and ISM) are presented in Fig. 12. The same power ratio to energy absorption is applicable for the on-body antennas. Based on this, the peak incident power should not exceed 0.25mW and 0.2mW for the ISM band and MISC band antennas, respectively.

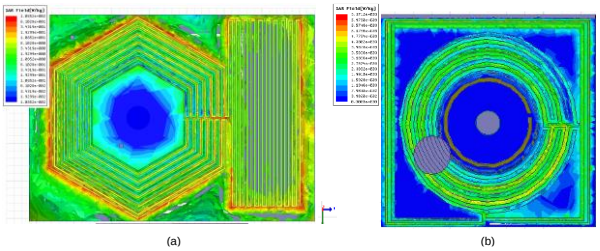

Fig. 12. Proposed on-body antenna showing the electromagnetic energy (SAR profile) distribution at (a) 400 MHz and (b) 2.4 GHz.

In addition to the dual band operation of the implant antenna, the analysis of path loss and propagation channel characteristics of WBAN is also a key research objective as the radio waves must travel from the implant antenna to on-body antennas through human tissue. S_{12} performance, the reverse transmission coefficient between the two antennas used to calculate coupling between antennas, was simulated for the MICS band on-body antenna design at multiple distances above the three-layer human tissue model for diversity reception with results presented in Fig. 13. The frequency behaviour of the S_{12} characteristics is considered to be as important as the S_{11} characteristics as this represents the wireless channel frequency response.

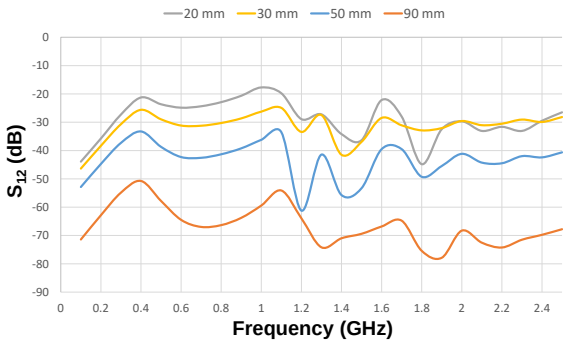

Fig. 13. S_{12} frequency response between the MICS band on-body antenna design and implant antenna at different distances 'd' between antennas.

It is well-known that large distances impose high path loss between implant and on-body antennas. As can be seen in Fig. 13, S_{12} for the MICS band on-body antenna varies from -20 dB to -50 dB as the on-body antenna moves from 90 mm to 2 mm between the three-layer tissue model.

S_{13} performance was also simulated for the ISM band on-body antenna design as shown in Fig. 14. It should be noted again that the ISM band on-body antenna was considered for the purpose of wake up the implant antenna for wireless telemetry transmission.

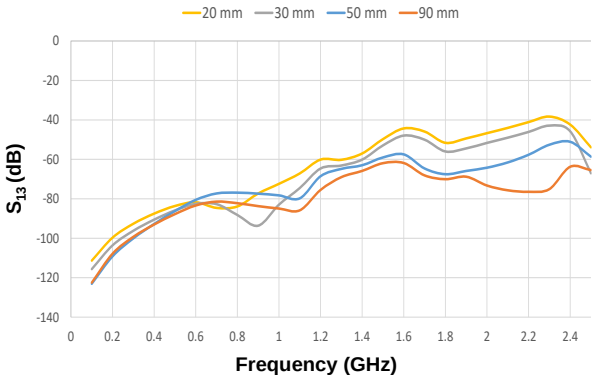

Fig. 14. Monitoring S_{13} characteristics between ISM band on-body antenna design and implant antenna at different distances *d* between antennas.

Figure 14 illustrates the coupling relationship between the in-body dual-band antenna and the ISM on-body antenna. The coupling between the two antennas at the ISM band is dampened compared to the MICS band shown in Fig. 13. This is due to the higher Q-factor experienced by patch antennas at higher frequencies resulting from increased surface wave excitation.

Analysis of the radiation efficiency and gain of the implant antenna suggests that both the gain and efficiency suffer largely as a result of being surrounded by the high-loss human tissue model. A comparison between the proposed implant antenna and other related published studies in terms of physical size, transmission bandwidth and peak gain (dB) is presented in Table 4.

Table 4: Comparison between implant antenna and related studies

Reference	Dimensions (mm x mm x mm)	Bandwidth ($\|S_{11}\|$ < -10 dB)	Peak Gain (dBi)
[11]	22.5 x 22.5 x 2.5 (1265.6 mm^3)	MICS	-2.4
		ISM	-7.5
[30]	16.5 x 16.5 X 2.54 (691.515 mm^3)	MICS	-31
		ISM	-9
[31]	13.4 x 16 x 0.835 (179 mm^3)	MICS	-30.6
		ISM	-19.1
[32]	10.02 x 10.02 x 0.675 (67.8 mm^3)	MICS	-30.5
		ISM	-19.2
[33]	8.75 x7.2 x 0.5 (31.5 mm^3)	MICS	-39.1
		ISM	-21.2
Proposed dual band design	6 x 5.7 x 1.3 (44.6 mm^3)	ISM	-22.7
		MICS	-39.8

The data presented in Table 4 shows that the proposed dual band implant antenna has the smallest physical dimensions and lower peak gain characteristics when compared to related studies. Low peak gain is observed due to the fact that the size reduction results as a less efficient radiator as compared to the λ/2 requirement. Generally, a reduction in antenna efficiency has a direct impact on antenna gain. Importantly, properties including phantom size, electric properties of the tissue model and the placement of implant antenna in tissue model may be differ between publications. Peak gain for the MICS band and ISM band on-body antennas were recorded as -35.6 dBi and -23 dBi, respectively. Low on-body antenna gains were anticipated due to the miniature size of the antennas. The design of low power implant antennas is crucial for patient safety and to eliminate interference with other systems. A maximum of -16 dBm effective radiated power may be used for implant devices in the MICS band in order to not interfere with the collocated Meteorological Aids Service band [33].

V. CONCLUSION

A miniaturized implant and two on-body antennas were proposed in this research study for wireless health monitoring with dual band operation. Hilbert fractal and serpentine radiator geometries were modified and characterized in order to benefit from space filling and self-similar properties. The implant antenna, and on-body MISC (402-405 MHz) and ISM (2.4-2.48 GHz) band antennas have dimensions 5.5 x 7.6 x 0.8 mm^3, 6 x 5.7 x 1.3 mm^3 and 5.8 x 5.5 x 0.8 mm^3 (width x height x thickness mm^3). The ISM band could be used to transmit the wake-up signal for the implant antenna while health monitoring could be completed over the MICS band. A proposed dual-band operation model was simulated in a 150 x 75 x 55 mm^3 four-layer tissue model (air, skin, fat and muscle) with satisfactory transmission characteristics (S_{11} below -15 dB). Zirconia material was used to achieve biocompatible characteristics while preventing a short-circuit between the antenna and human tissue. A coaxial probe will be used as a feeding line for future experimental analysis and a shorting pin was used to connect the radiating elements to the ground plane in order to achieve resonance at specific frequencies. Analysis demonstrated that the implant and on-body antennas have satisfactory, omni-directional S_{12} and S_{13} transmission characteristics and acceptable SAR results were achieved for dual-band operation. The achievement of stable transmission properties with antennas that are notably smaller than those presented in previous studies is a significant achievement of this work.

REFERENCES

[1] A. Kiourti and K. S. Nikita, "A review of implantable patch antennas for biomedical telemetry: Challenges and solutions," *IEEE Trans. Antennas Propag*., vol. 54, pp. 210-228, 2012.

[2] A. Ahmed, T. Kalsoom, M. Rehman, N. Ramzan, S. Karim, and Q. Abbasi, "Design and study of a small implantable antenna design for blood glucose monitoring," *Appl. Comput. Electrom.*, vol. 33, no. 10, pp. 1146-1151, 2018.

[3] Y. Hao, A. Alomainy, P. S. Hall, Y. I. Nechayev, C. G. Parini, and C. C Constantinou, "Antennas and propagation for body-centric wireless communications," *IEEE/ACES International Conference on Wireless Communications and Applied Computational Electromagnetics*, 2005. 10.1109/WCACEM.2005.1469656

[4] C. M. Furse, "Biomedical telemetry: Today's opportunities and challenges," *IEEE Workshop on Antenna Technology Small Antennas and Novel Metamaterials*, Santa Monica, CA, 2009. 10.1109/ IWAT.2009.4906963.

[5] J. Kim and Y. Rahmat-Samii, "Implanted antennas inside a human body: Simulations, designs, and characterizations," *IEEE Trans. Microw. Theory Tech.*, vol. 52, pp. 1934–1943, 2004.

[6] P. Soontornpipit, C. M. Furse, and Y. C. Chung, "Design of implantable micro strip antennas for communication with medical implants," *IEEE Trans. Microw. Theory Tech*., vol. 52, pp. 1944-1951, 2004.

[7] P. Soontornpipit, C. M. Furse, and Y. C. Chung, "Miniaturized biocompatible micro strip antenna using genetic algorithm," *IEEE Trans. Antennas Propag.*, vol. 53, pp. 1939-1945, 2005.

[8] C. M. Lee, T. C. Yo, F. J. Huang, and C. H. Luo, "Dual-resonant Pi-shape with double L-strips PIFA for implantable biotelemetry," *Electron. Lett*., vol. 44, pp. 837-838, 2008.

[9] A. O. Kaka, M. Toycan, and S. D. Walker, "Miniaturized stacked implant antenna design at ISM band with biocompatible characteristics," *COMPEL*, vol. 34, pp. 1270-1285, 2015.

[10] Federal Communications Commission, "§ 95.628 Med radio transmitters in the 413-419 MHz, 426-432 MHz, 438-444 MHz, and 451-457 MHz and 2360-2400 MHz bands," in "Code of Federal Regulations, Title 47—Telecommunication, Chapter 1—FCC, Subchapter D-Safety and Special Radio Services, Part 95—Personal Radio Services, Subpart E—Technical Regulations," Tech. Rep. 95.628, 2012.

[11] T. Karacolak, A. Z. Hood, and E. Topsakal, "Design of a dual-band implantable antenna and development of skin mimicking gels for continuous glucose monitoring," *IEEE Trans. Microw. Theory Tech.*, vol. 56, pp. 1001-1008, 2008.

[12] C. J. Sańchez-Fernańdez, O. Quevedo-Teruel, J. Requena-Carrión, L. Inclań-Sańchez, and E. Rajo-

Iglesias, "Dual-band micro strip patch antenna based on short-circuited ring and spiral resonators for implantable medical devices," *IET Microw. Antenna P.*, vol. 4, pp. 1048-1055, 2010.
[13] T. Karacolak, R. Coope, J. Butler, S. Fisher, and E. Topsakal, "In vivo verification of implantable antennas using rats as model animals," *IEEE Antennas Wirel. Propag. Lett.*, vol. 9, pp. 334-337, 2010.
[14] Z. G. Liu and Y. X. Guo, "Dual band low profile antenna for body centric communications," *IEEE Trans. Antennas Propag.*, vol. 61, pp. 2282-2285, 2013.
[15] B. Sanz-Izquierdo, J. A. Miller, J. C. Batchelor, and M. I. Sobhy, "Dualband wearable metallic button antennas and transmission in body area networks," *IET Microw Antenna P.*, vol. 4, pp. 182-190, 2010.
[16] P. J. Soh, G. A. E. Vandenbosch, S. L. Ooi, and M. R. N. Husna, "Wearable dual-band Sierpinski fractal PIFA using conductive fabric," *Electron. Lett.*, vol. 47, pp. 365-367, 2011.
[17] P. J. Soh, G. A. E. Vandenbosch, S. L. Ooi, and N. M. A. Rais, "Design of a broadband all-textile slotted PIFA," *IEEE Trans. Antennas Propag.*, vol. 60, pp. 379-384, 2012.
[18] S. Agneessens and H. Rogier, "Compact half diamond dual-band textile HMSIW on-body antenna," *IEEE Trans. Antennas Propag.*, vol. 62, pp. 2374-2381, 2014.
[19] B. Y. Toh, R. Cahill, and V. F. Fusco, "Understanding and measuring circular polarization," *IEEE T. Educ.*, vol. 46, pp. 313-318, 2013.
[20] C. P. Deng, X. Y. Liu, Z. K. Zhang, and M. M. Tentzeris, "A miniascape-like triple-band monopole antenna for WBAN applications," *IEEE Antennas Wirel. Propag. Lett.*, vol. 11, pp. 1330-1333, 2012.
[21] G. K. Mkongwa, L. Qingling, and Z. Chaozhu, "Design of the Tri-band UWB microstrip patch antenna for WBAN applications," *Appl. Comput. Electrom.*, vol. 38, pp. 1305-1311, 2019.
[22] S. Zhu and R. Langley, "Dual-band wearable antenna over EBG substrate," *Electron. Lett.*, vol. 43, pp. 141-143, 2007.
[23] S. Zhu and R. Langley, "Dual-band wearable textile antenna on an EBG substrate," *IEEE Trans. Antennas Propag.*, vol. 57, pp. 926-935, 2009.
[24] H. R. Raad, A. I. Abbosh, H. M. Al-Rizzo, and D. G. Rucker, "Flexible and compact AMC based antenna for telemedicine applications," *IEEE Trans. Antennas Propag.*, vol. 61, pp. 524-531, 2013.
[25] N. Chahat, M. Zhadobov, R. Sauleau, and K. Mahdjoubi, "Improvement of the on-body performance of a dual-band textile antenna using an EBG structure," *2010 Loughborough Antennas & Propagation Conference*, pp. 465-468, 2010. 10.1109/LAPC.2010.5666201.
[26] M. Mantash, A. C. Tarot, S. Collardey, and K. Mahdjoubi, "Dual-band CPW-fed G-antenna using an EBG structure," *2010 Loughborough Antennas & Propagation Conference*, pp. 453-456, 2010. 10.1109/LAPC.2010.5666211.
[27] A. O. Kaka, M. Toycan, V. Bashiry, and S. D. Walker, "Modified Hilbert fractal geometry, multi-service, miniaturized patch antenna for UWB wireless communication," *COMPEL*, vol. 6, pp. 1835-1849, 2012.
[28] W. Xia, K. Saito, M. Takahashi, and K. Ito, "Performances of an implanted cavity slot antenna embedded in the human arm," *IEEE Trans. Antennas Propag.*, vol. 57, pp. 894-898, 2009.
[29] Federal Communications Commission Office of Engineering and Technology (2001) Evaluating compliance with FCC guidelines for human exposure to radio frequency electromagnetic fields. upplement C: Additional information for evaluating compliance of mobile and portable devices with FCC limits for human exposure to radio frequency emissions.
[30] C. Liu, S. Xiao, Y. X. Guo, Y. Y. Bai, M. C. Tang, and B. Z. Wang, "Compact circularly-polarized microstrip antenna with symmetric-slit," *Electron. Lett.*, vol. 48, pp. 195-196, 2012.
[31] Z. Duan, Y. X. Guo, M. Je, and D. L. Kwong, "Design and in vitro test of a differentially fed dual-band implantable antenna operating at MICS and ISM bands," *IEEE Trans. Antennas Propag.*, vol. 62, pp. 2430-2439, 2014.
[31] L. J. Xu, Y. X. Guo, and W. Wu, "Miniaturized dual-band antenna for implantable wireless communications," *IEEE Antennas Wirel. Propag. Lett.*, vol. 13, pp. 1160-1163, 2014.
[32] Y. Cho and H. Yoo, "Miniaturized dual-band implantable antenna for wireless biotelemetry," *Electron. Lett.*, vol. 52, pp. 1005-1007, 2016.
[33] "International Telecommunications Union-Radio communications (ITU-R), Radio Regulations, SA.1346," ITU, Geneva, Switzerland; available online: http://itu.int/home

Ademola O. Kaka received his OND and HND degrees from the Department of Electrical and Electronic Engineering of Yaba College of Technology, Nigeria in 2008. He has received his M.Sc. and Ph.D. degrees from the Department of Electrical & Electronic Engineering and the department of Computer Engineering of Cyprus International University, North Cyprus in 2012

and 2016 respectively. His research interests include miniaturized, biocompatible and low loss implant antenna designs and their applications in wireless communication systems.

Mehmet Toycan received his B.Sc. degree from the Department of Electric and Electronic Engineering, Eastern Mediterranean University, in 2004. He received the M.Sc. degree in Telecommunications & Information systems and Ph.D. degree in Electronics from University of Essex, Colchester, U.K, in 2005 and 2009 respectively. During his Ph.D. degree, he was a member of Access Networks Laboratory, department of Computer and Electronic Systems at University of Essex. He was also involved in the Network of Excellence, BONE-project ("Building the Future Optical Network in Europe") where he was collaborating with groups from other universities to develop efficient, low-cost optical access network architectures. He is currently working as a Full-time Lecturer and the Director of Communication Technologies Research Centre in Cyprus International University. His research interests are in the fields of cost and energy efficient, scalable optical access networks for FTTH scenarios featuring wireless communication transmission and implant antenna designs for wireless health monitoring applications. In addition, his information systems research team is recently working on electronic health solutions for developing countries.

Stuart D. Walker was born in Dover, UK in 1952. He received the B.Sc. (Hons) degree in Physics from Manchester University, Manchester, UK, in 1973, the M.Sc. degree in Telecommunications Systems and Ph.D. degree in Electronics from Essex University, Colchester, UK, in 1975 and 1981, respectively. He is currently a Full Professor at Essex University where his main research interest is access networks. He has been involved in many EPSRC and European Union research projects over the years, recent examples being BONE, MUSE-I and II, UROOF, STRONGEST, FIVER and OASE. He has published over 250 peer-reviewed journal and conference papers and holds four patents.

Doğa Kavaz received her B.Sc. degree from the Department of Chemistry, Hacettepe University in 2006. She received the M.Sc. degree in Biochemistry (Chemistry) and Ph.D. degree in Nanotechnology (Chemistry) from Hacettepe University, in 2009 and 2013. During her Ph.D. she went to Harvard University as a Researcher for 1 year with a scholarship from TUBITAK. She took part in a joint project with various universities and developed biomaterials for use in tissue engineering. She is currently working as a Full-time Lecturer and Researcher of Biotechnology Research Centre in Cyprus International University. Her research interests include the development and characterization of biomedical materials to be used in medical purposes.